IEEE Access
Multidisciplinary | Rapid Review | Open Access Journal

Received June 30, 2019, accepted July 16, 2019, date of publication July 23, 2019, date of current version August 8, 2019.

Digital Object Identifier 10.1109/ACCESS.2019.2930687

Meta-Surface Antenna Array Decoupling Designs for Two Linear Polarized Antennas Coupled in H-Plane and E-Plane

JIAYIN GUO[1], (Student Member, IEEE), FENG LIU[1], (Student Member, IEEE), LUYU ZHAO[1], (Senior Member, IEEE), YINGZENG YIN[1], GUAN-LONG HUANG[2], (Senior Member, IEEE), AND YINGSONG LI[3,4], (Senior Member, IEEE)

[1]Key Laboratory of Antennas and Microwave Technologies, Xidian University, Xi'an 710071, China
[2]Guangdong Provincial Mobile Terminal Microwave and Millimeter-Wave Antenna Engineering Research Center, College of Information Engineering, Shenzhen University, Shenzhen 518060, China
[3]College of Information and Communication Engineering, Harbin Engineering University, Harbin 150001, China
[4]Key Laboratory of Microwave Remote Sensing, National Space Science Center, CAS, Beijing 100190, China

Corresponding author: Luyu Zhao (lyzhao@xidian.edu.cn)

This work was supported by the National Natural Science Foundation of China under Grant 61701366 and Grant 61801300.

ABSTRACT In this paper, meta-surface superstrates are used to decouple two linear polarized antennas coupled in H-plane and E-plane, respectively. By properly designing the geometry of the double layer short wires as the unit cell of the meta-surface, as well as the height of the meta-superstrate, two linearly polarized antennas can be decoupled in H-plane and E-plane, respectively. Both the antenna pairs coupled in E- and H-planes with and without meta-surfaces are fabricated and measured. The results demonstrate that the antennas with the meta-surface superstrate are able to operate in the band of 3.3–3.7 GHz with reflection better than −15 dB and the isolation can be improved from 10 to 25 dB in the H-plane case and can be improved from 15 to 30 dB in the E-plane case. Such decoupling method can be applied extensively in 5G base stations where size constraints are becoming stringent.

INDEX TERMS Antenna array decoupling, base station, metamaterial, meta-surface, mutual coupling, 5G communication systems.

I. INTRODUCTION

Nowadays, the fifth generation of mobile communication technology (5G) has become the main stream technology for mobile communication systems, which requires higher transmission rate on a wider operation bandwidth. Therefore, the antenna array will play an important supporting role in meeting the capacity and coverage requirements of the 5G system, as one of the most important technical means to improve the spectrum efficiency of the system.

The antenna technology for 5G base stations is evolving very fast, and they have to meet the requirements of antenna miniaturization, wide frequency band, high isolation, etc. Therefore, while satisfying the antenna matching, the antenna decoupling is an important concern when designing the base station antenna in a compact volume. There has been a lot of literature on the decoupling design of antennas in recent years and these papers can be divided into the following categories:

1) Neutralization line and decoupling network [1]–[11]: These decoupling networks or neutralization lines are designed between antennas to reduce their mutual couplings.

2) Ground plane modification design [12]–[18], which can accomplish high isolation by cutting slots on the ground plane.

3) Characteristic mode based design [19]–[24]: For example, in [20], high isolation is achieved by designing orthogonal radiation patterns.

4) Parasitic elements based design [25]–[27]: It can be seen in [27] that a thin surface composed of a plurality of electrical small metal patches is designed to reduce the mutual coupling between antenna elements.

In recent years, metamaterial based or inspired decoupling design has been more and more popular [28]–[36], which can be further divided into the following three types of methods:

The associate editor coordinating the review of this manuscript and approving it for publication was Mohammad Tariqul Islam.

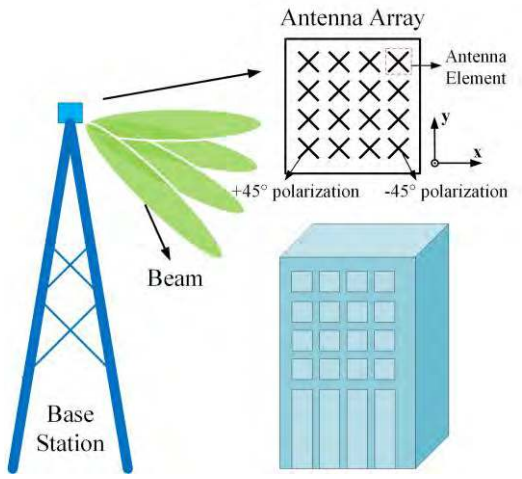

FIGURE 1. Schematic diagram of the arrangement of base station antenna.

First of all, the Electromagnetic Band Gap (EBG) structure [28]–[30] is inserted between antennas to reduce mutual coupling. Using the EBG structure as a decoupling solution first appeared in [28]. It is proved that this structure has the characteristics of suppressing surface waves. Later [29] proves that EBG is also effective at millimeter wave bands.

Secondly, the meta-cloak/wall [31]–[33] inserted vertically between the antenna elements can also be used to reduce coupling. A novel metamaterial polarization-rotator (MPR) wall is proposed for reducing the mutual coupling between millimeter-wave dielectric resonator antennas (DRAs) coupled in H-plane [33].

Finally, the meta-surface superstrate decoupling method has become more and more popular these days [34]–[36]. In [34], a two-layer transmission-type frequency selective surface (FSS) superstrate which consists of planar crossed-dipole metal strips is proposed for circular polarized MIMO antennas. In [35], the decoupling superstrate is composed of periodic square split ring resonators (SRRs). An updated and compact version of the meta-superstrate is given in [36], solving the coupling of two antennas in the H-plane.

Most of the previously mentioned meta-surface superstrate deal with the mutual coupling in H-plane, yet in real-world base station applications as shown in Fig. 1, both H-coupling and E-coupling exist. The purpose of this paper is to investigate the capabilities of the meta-surface superstrate to mitigate the coupling between two antennas aligned in H-plane and E-plane, respectively.

The rest of the paper will be organized as follows: The design and analysis of the meta-surface antenna array decoupling (MAAD) method for antenna array arranged along the H-plane are given in section II. In section III, the design and discussion of the MAAD method for antenna array arranged along the E-plane are displayed, then comparison and analysis of the results in both cases will also be given. Conclusions are made in section IV.

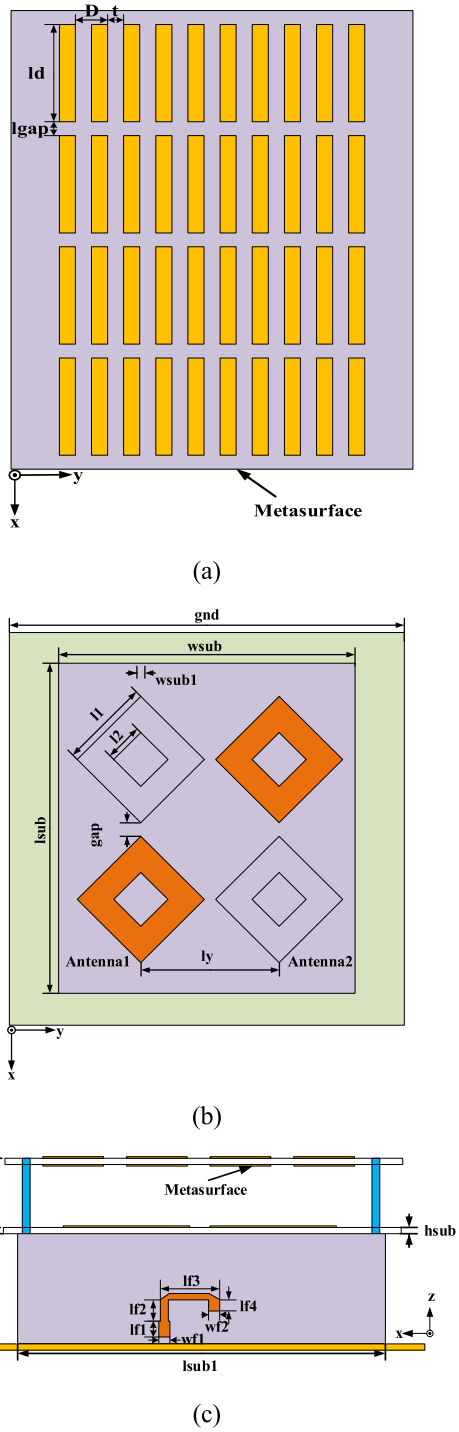

FIGURE 2. Configuration of the proposed SRD antenna. (a) Top view of the proposed meta-surface. (b) Top view of the antenna array without meta-surface. (c) Side view of the SRD antenna with Γ-probe feed structure.

II. MAAD DESIGN FOR ANTENNAS COUPLED IN THE H-PLANE

A meta-surface of double-layer short wires is used as the superstrate for two antennas coupled in H-plane in order to improve the isolation between the antennas while maintaining the matching performance within the desired band. Fig. 2 shows the configuration of the proposed antenna array,

TABLE 1. Key parameters of the proposed SRD antenna array arranged along the H-Plane (UNIT: mm).

Variable	Value	Variable	Value
gnd	100	lf3	12
wsub	77	lf4	4.5
wsub1	1	wf2	2
lsub	81	hsub1	22
l1	21	hsub	1
l2	7	hgap	15
gap	4.5	ld	15.3
wf1	3.4	lgap	4.5
lf1	4	t	3
lf2	6	D	7

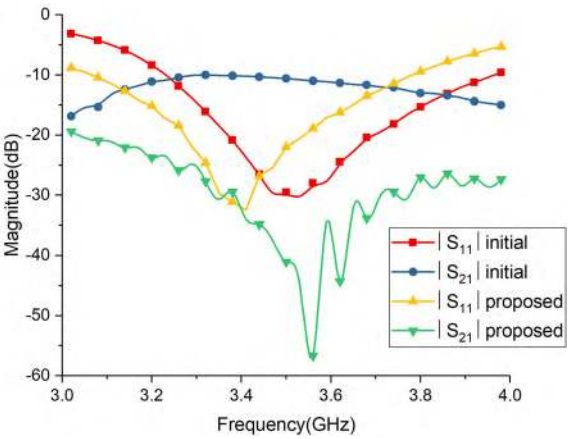

FIGURE 3. Measured S-parameters of the initial antenna (without meta-surface) and proposed antenna (with meta-surface) arranged along the H-plane.

which is arranged along the y-axis. The proposed antenna consists of two ring-shaped antenna elements, a metalized ground plane, feeding networks, and a meta-surface superstrate. The square ring-shaped dipole (SRD) is printed on a FR4 substrate. And the Γ-shaped feed structure is etched on one side of another FR4 substrate. The two rectangular metal plates printed on the other side of the FR4 substrate are shorted to the ground plane. All the FR4 substrates have a thickness of 1 mm while the relative dielectric constant is 4.4 and the loss tangent is 0.02. The meta-surface is etched on the F4B substrate with a thickness of 0.8 mm, whose relative dielectric constant is 2.65. The center to center distance of the two antennas along the y-axis is 30 mm, which is about 0.35 wavelengths at 3.5 GHz. Other design parameters are shown in Table 1. The SRD antenna array is designed using ANSYS HFSS software.

In order to better illustrate the decoupling mechanism, the comparisons between the antenna arrays without meta-surface (coupled) and with the designed meta-surface (decoupled) are given in this section. The measured S-parameters of the coupled and decoupled antenna array are shown in Fig. 3. It can be clearly seen that $|S_{21}|$ is significantly reduced from −10 dB to below −25 dB within

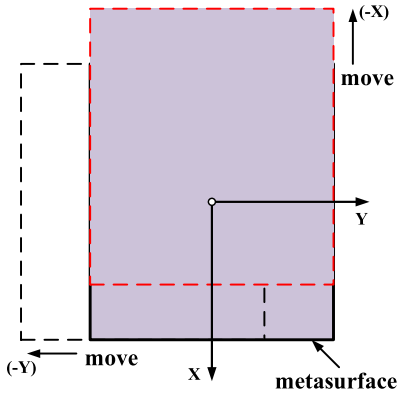

FIGURE 4. The displacement sensitivity analysis model.

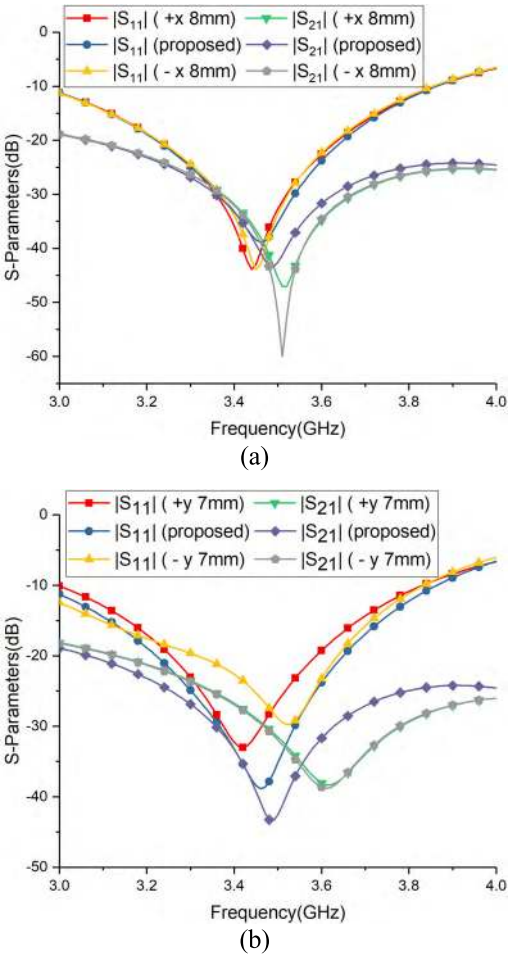

FIGURE 5. Effect of displacement along the (a) x axis; (b) y axis on S-parameters of the antennas coupled in H-plane with the meta-surface.

the band of 3.3 −3.7 GHz while $|S_{11}|$ is maintained to be below −15 dB.

Then, the designed meta-surface superstrate is moved a certain distance along the x and y axis to observe the sensitivity of the design to superstrate displacement as shown in Fig. 4. Fig. 5 (a) shows the simulated results of the meta-surface moving 8 mm (10% of the length of the meta-surface) along the positive and negative directions of

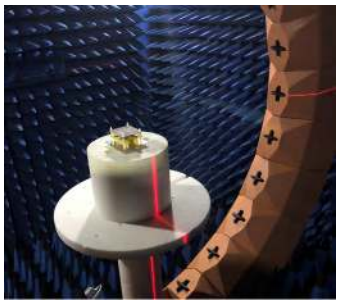

FIGURE 6. The photograph of antenna prototype under test in anechoic chamber.

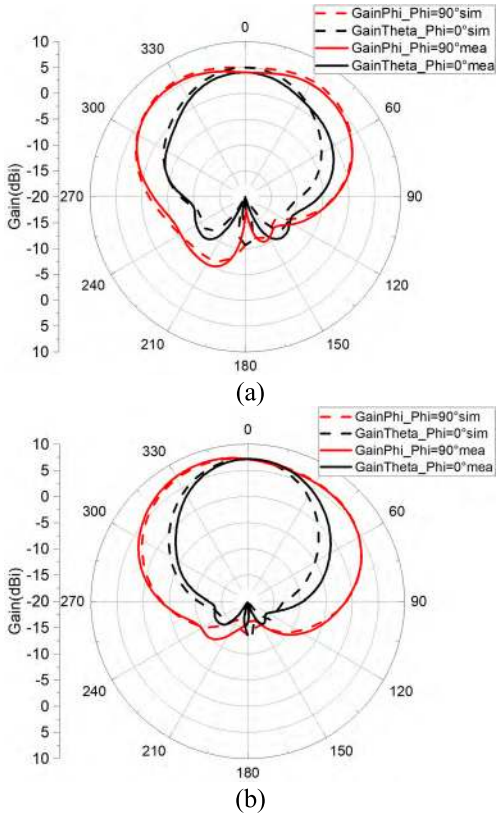

FIGURE 7. Simulated and Measured radiation patterns of the two antennas at 3.5 GHz (a) without and; (b) with meta-surface.

the x axis, respectively. It has little effect on the return loss and isolation of the antennas. Fig. 5 (b) shows the simulated results of the 7 mm (10% of the width of the meta-surface) displacement of the meta-surface along the positive and negative directions along the y axis, respectively. A slight yet acceptable frequency shift is observed in Fig. 5 (b).

The radiation characteristics of the antenna array with and without meta-surface are evaluated in a 24-probe near field anechoic chamber as shown in Fig. 6. The simulated and measured radiation patterns at 3.5 GHz are plotted in Fig. 7, where (a) is the pattern of the coupled antenna array without meta-surface, and (b) is the pattern of the decoupled antenna array with the designed meta-surface. During the measurement, the port of the antenna 2 is terminated with a matched load when antenna 1 is excited and vice versa. For the sake

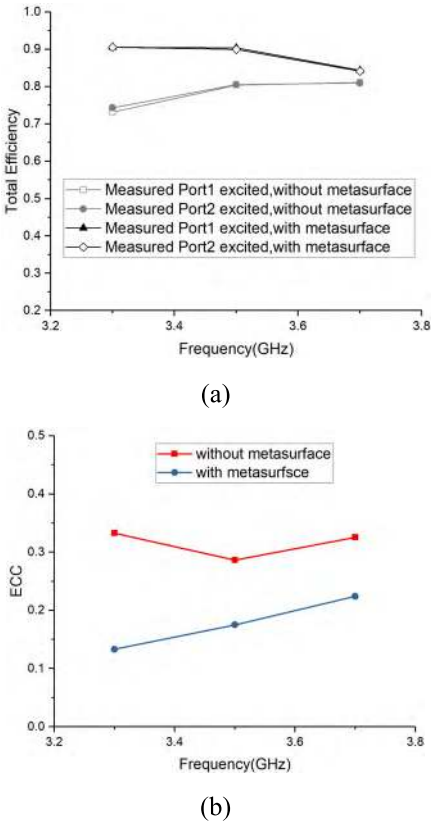

FIGURE 8. Measured (a) total efficiencies, and (b) ECCs for the two antennas without and with meta-surface.

of simplicity, we only give the radiation patterns when port 1 is excited because of the symmetrical antenna structure. It can be observed that the results of the simulated and measured radiation patterns are in good agreement from Fig. 7. The gain of the proposed antenna array can reach 7.2 dBi at the boresight, and is improved by 2 dB compared to the coupled antenna array.

The measured total efficiencies of the antennas with and without meta-surface are also compared in Fig. 8 (a). It shows that the efficiency is improved by 10% with the meta-surface introduced. It is well known that the envelop correlation coefficient (ECC) is also a very important figure of metric in multiple antenna systems. Therefore, the calculation results of ECC based on measured radiation patterns are given in Fig. 8 (b). Compared with the initial antenna array without meta-surface, the ECC of the proposed antenna array with meta-surface decreases from about 0.3 to about 0.15 in the frequency band of interest. The increase of antenna efficiency and the decrease of ECC prove the benefit of the meta-surface superstrate.

III. MAAD DESIGN FOR ANTENNAS COUPLED IN THE E-PLANE

A. PROPOSED ANTENNA DESIGN

The MAAD design for antennas coupled in the E-plane will be discussed in this section. The comparisons between antenna array without meta-surface (initial antenna array)

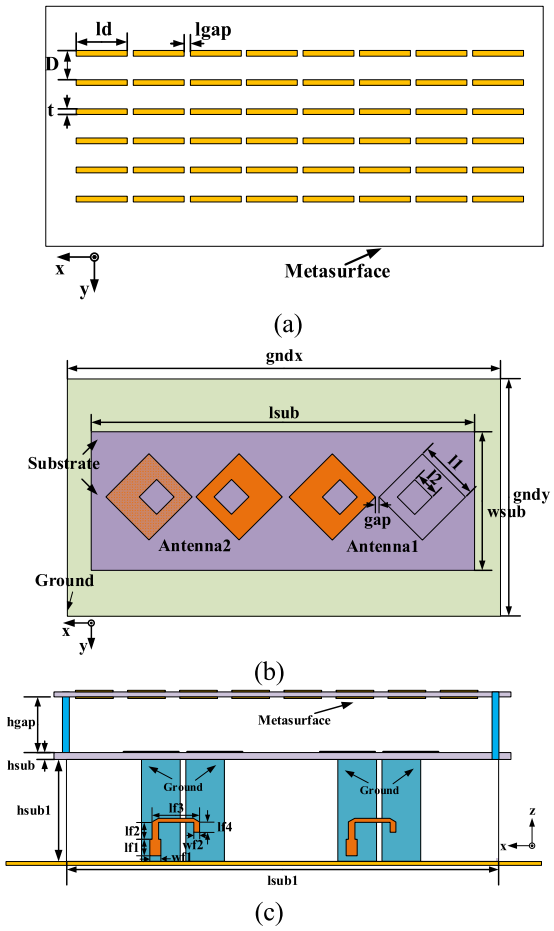

FIGURE 9. Configuration of the proposed SRD antenna array arranged along the E plane. (a) Top view of the proposed meta-surface. (b) Top view of the antenna array without meta-surface. (c) Side view of the SRD antenna with Γ-probe feed structure.

TABLE 2. Key parameters of the proposed SRD antenna arranged along the E-Plane (UNIT: mm).

Variable	Value	Variable	Value
gndx	200	lf3	10.5
gndy	100	lf4	4.5
wsub	60	wf2	3.2
lsub	170	hsub1	21.3
l1	24	hsub	1
l2	8	hgap	8.2
gap	3	ld	16.6
wf1	3.2	lgap	1.5
lf1	5.9	t	1
lf2	6	D	8

and with meta-surface (proposed antenna array) are investigated to better understand the decoupling mechanism. The designed antenna is shown in Fig. 9, which has a similar structure as the antenna array arranged along the H-plane. The structure of the coupled antenna array is almost the same as that of the proposed antenna array except for the absence of the meta-surface. The key design parameters of the antenna array and meta-surface are listed in Table 2.

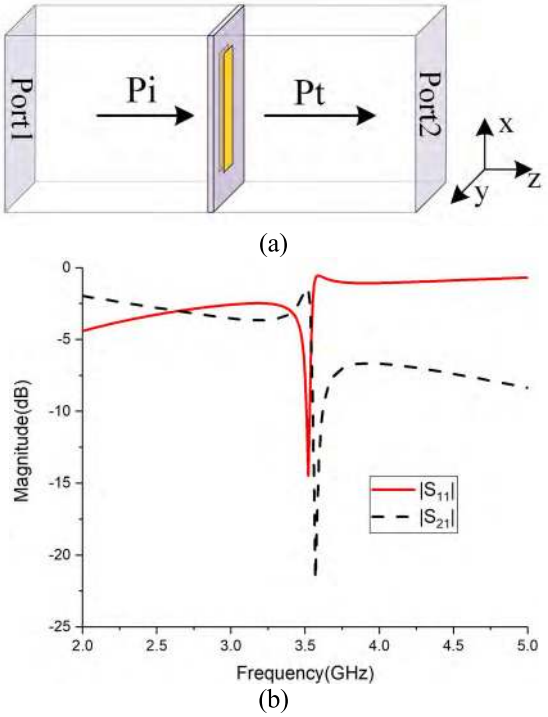

FIGURE 10. (a) The unit structure of the meta-surface. (b) The S-parameter simulation results of unit cell of the meta-surface.

In order to better understand the decoupling function of meta-surface, the unit structure of meta-surface is analyzed as shown in Fig. 10 (a). In this simulation, both ports are excited by FloquetPort. Moreover, the master-slave boundary conditions are adopted to facilitate the periodic simulation of a unit. The simulation results of S-parameter are shown in Fig. 10 (b). It can be seen that the unit of meta-surface can resonate at about 3.5 GHz. Furthermore, the size of the unit can be adjusted to change its resonance frequency according to the requirement.

Fig. 11 shows the comparison of the initial antenna array and the proposed antenna array with respect to the measured S-parameters. It can be seen that the isolation of the antenna array is approximately 15 dB between 3.3 GHz and 3.7 GHz without loading meta-surface. The $|S_{21}|$ can be reduced to around -30 dB in the desired frequency band with the meta-surface superstrate introduced. In other words, the isolation is improved more than 15 dB across the entire frequency band of interest. In addition, the antenna array remains good impedance matching within the band of 3.3 $-$3.7 GHz

The comparisons of the simulated and measured results on S-parameters are shown in Fig. 12. It is obvious that the simulated results of the S parameters are consistent with the measured ones.

B. PARAMETRIC ANALYSIS

In order to understand the design sensitivity, the key parameters of the meta-surface superstrate affecting the mutual coupling between antennas have been analyzed, including the length *ld* of the meta-surface unit and the height *hgap* from the

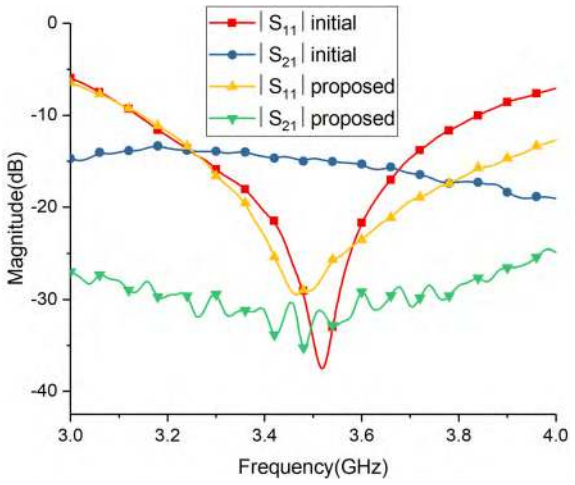

FIGURE 11. Measured S-parameters of the initial antenna (without meta-surface) and proposed antenna (with meta-surface) arranged along the E-plane.

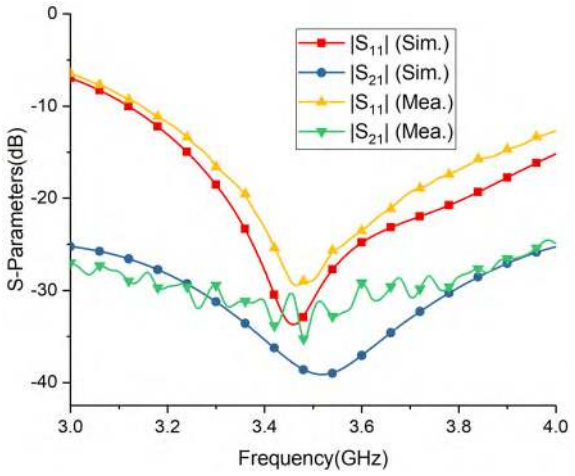

FIGURE 12. Comparison of the simulated and measured results.

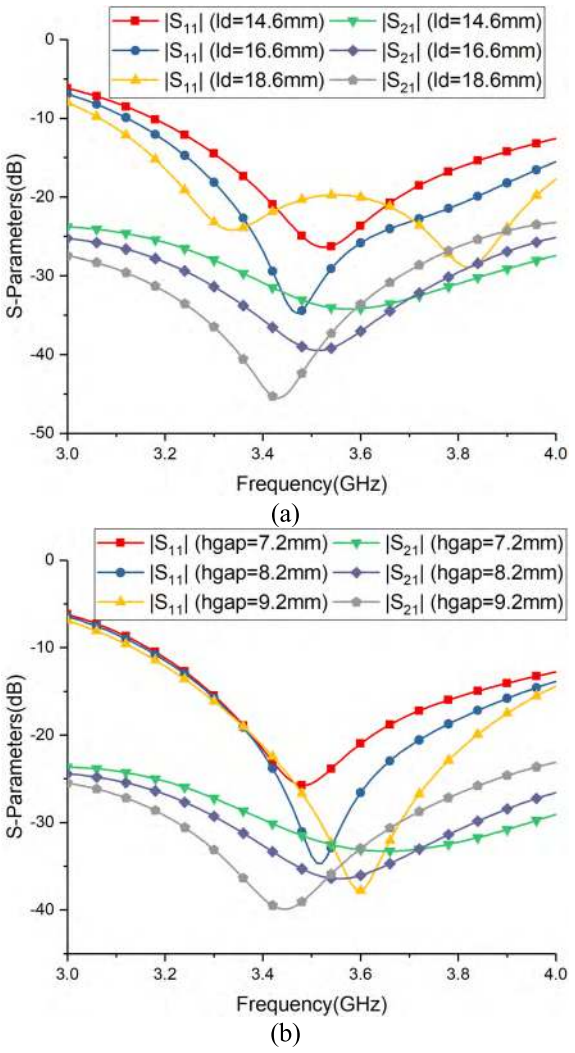

FIGURE 13. Simulated S-parameters versus (a) the parameter ld; (b) the parameter hgap.

meta-surface to the initial antenna array. When one parameter on the decoupling effect is studied, the other parameters remain the same as that in Table 2.

Fig. 13 (a) displays the effect of the parameter *ld* on the S-parameters. It can be observed that when the meta-surface unit length *ld* increases, the matching bandwidth increases accordingly. Meanwhile, the overall trend of the curve moves to the left and down. Therefore, the parameter *ld* is chosen to be 16.6 mm in order to leverage matching and decoupling performances.

Fig. 13 (b) shows the effect of the parameter *hgap* on the S-Parameters. As can be seen, when the *hgap* increases, the resonant frequency of the $|S_{11}|$ shifts to the high-frequency band and the matching performance becomes better gradually. Moreover, the overall trend of the curve moves to the left and down as the *hgap* increases. Parameter *hgap* is finally determined to be 8.2 mm for the best matching and decoupling performances.

In addition, some other parameters of the design, such as the width of the meta-surface unit, the lateral misalignment, and longitudinal misalignment have also been studied and the simulation shows they have a relatively negligible effect on the matching and decoupling performance of the antennas.

In order to study the influence of the misplacement of the meta-surface on the overall antenna performance, the meta-surface is moved by a certain distance along the x and y axis. While keeping the other parameters of the antenna unchanged, the meta-surface is moved 15 mm (10% of the length of the meta-surface) along the $+$x and $-$x axis respectively. The simulation results are shown in Fig. 14 (a). It is clear from Fig. 14 (a) that the movement of the meta-surface along the x axis has little effect on return loss and isolation. Fig. 14 (b) shows the result of the meta-surface moving 5 mm (10% of the width of the meta-surface) along the $+$y and $-$y axis, respectively. The results show that the impedance bandwidth remains essentially the same as the meta-surface moves along the y axis, but the movement of the meta-surface along the y axis has a relatively larger effect on the isolation. Nevertheless, it still meets the requirements of $|S_{21}| < -25$ dB.

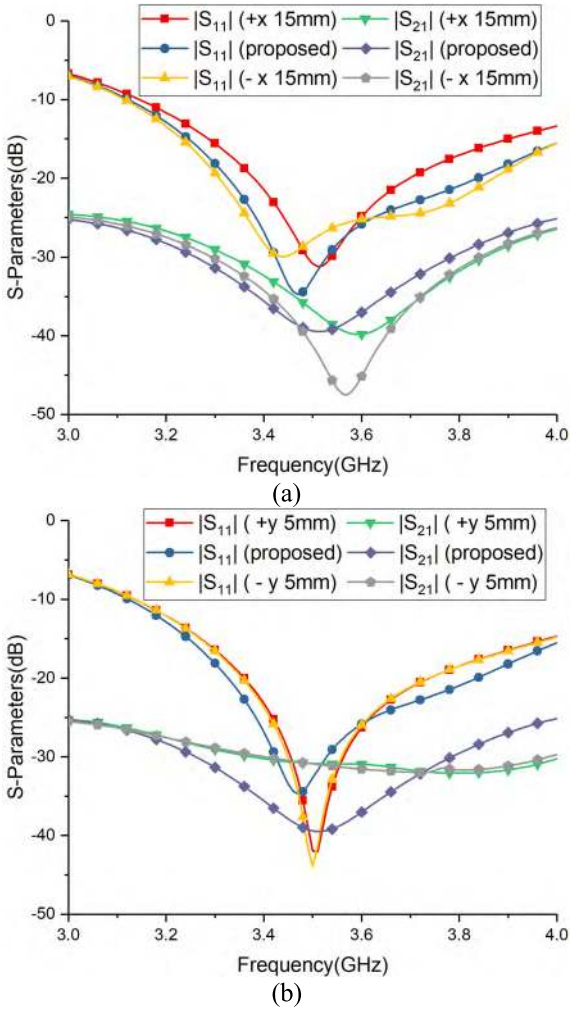

FIGURE 14. Effect of displacement along the (a) x axis; (b) y axis on S-parameters of the antennas coupled in E-plane with the meta-surface.

C. FIELD DISTRIBUTION

To further investigate the decoupling mechanism, the electric field distribution and magnetic field distribution of the antenna array when port 1 is excited are plotted in Fig. 15 and Fig. 16, respectively. Fig. 15 (b) shows the electric field distribution of the decoupled antenna array, and the electric field distribution of the coupled antenna array is given as a reference in Fig. 15 (a). By comparing the electric field distributions of Fig. 15 (a) and 15 (b), it can be obviously seen that almost no electric field is coupled to port 2 when the port1 of the antenna is excited after loading the meta-surface superstrate. This indicates that the field distribution can be suppressed well in a fixed area and can be prevented from being coupled to another antenna. The same conclusion can be drawn from the magnetic field.

In order to better explain the effect of meta-surface on improving isolation, the amplitude distribution of the electric field of the two antennas (the coupled antenna and the decoupled antenna) is shown in Fig. 17. It can be clearly seen that the field radiated by antenna 1 is more bound around the meta-surface and radiates into space instead of coupling to

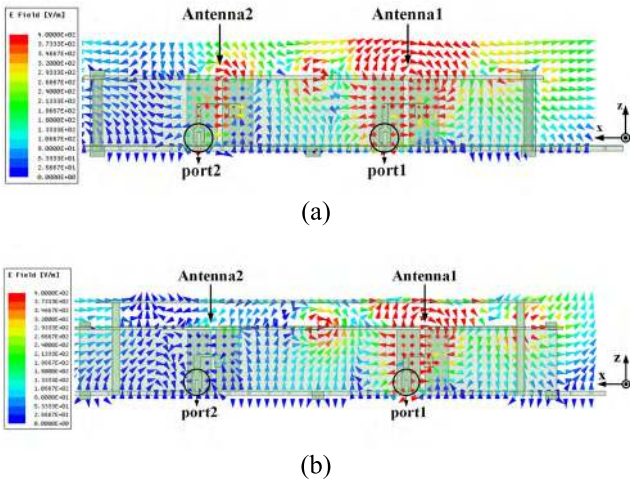

FIGURE 15. Vector distribution of electric field when port 1 is excited for (a) coupled antenna; (b) decoupled antenna.

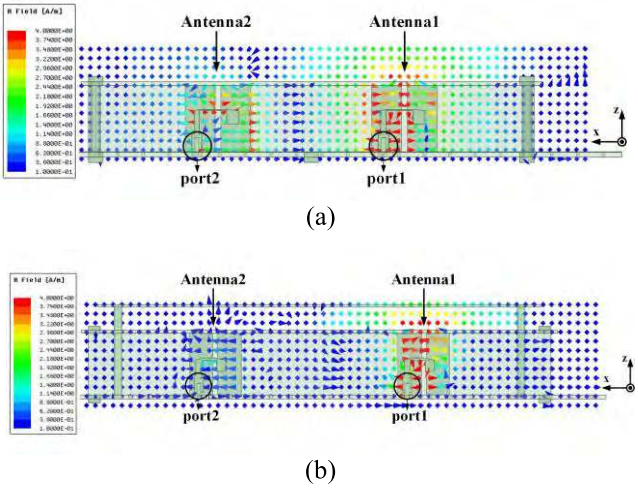

FIGURE 16. Vector distribution of magnetic field when port 1 is excited for (a) coupled antenna; (b) decoupled antenna.

antenna 2 with loading the meta-surface. Therefore, the isolation between the two antenna ports has been significantly improved.

D. RADIATION PATTERNS

The fabricated antennas, as well as the configuration of the radiation measurement, is shown in Fig. 18. Fig. 19 shows the simulated and measured radiation patterns of antenna array with and without meta-surface at 3.5 GHz. For the sake of simplicity, only the radiation patterns are displayed while port 1 is excited. As can be seen, the measured and simulated radiation patterns still maintain good consistency. It can be noticed that the gain of the decoupled antenna at the boresight is 7.2 dBi, which is 1.5 dB more than the one of antenna array without meta-surface.

The measured radiation patterns of the two antenna arrays with and without meta-surface at three different frequencies (3.3 GHz, 3.5 GHz, and 3.7 GHz) are depicted in Fig. 20,

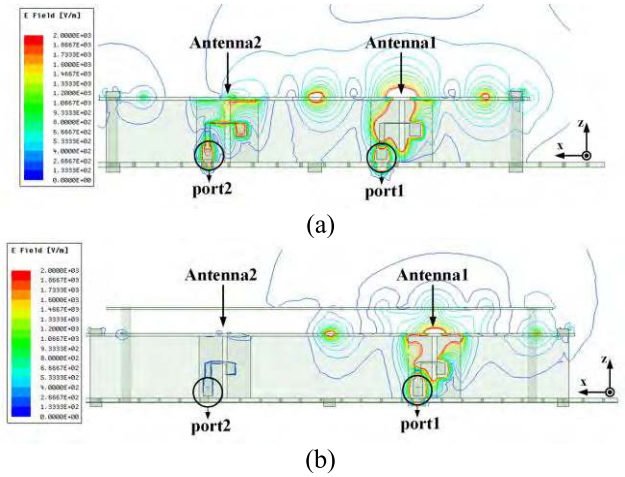

FIGURE 17. Amplitude distribution of electric field when port 1 is excited for (a) coupled antenna; (b) decoupled antenna.

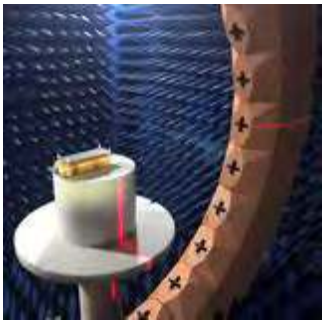

FIGURE 18. The photograph of antenna prototype under test in anechoic chamber.

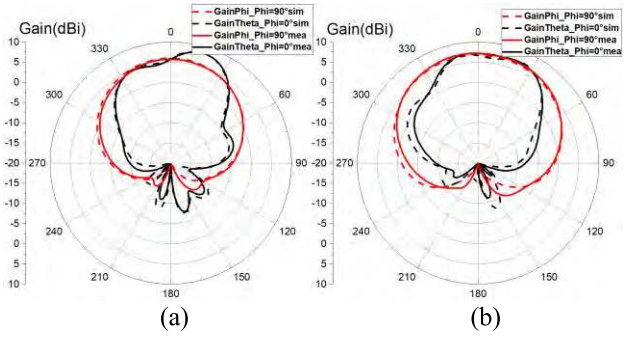

FIGURE 19. Simulated and Measured radiation patterns of the two antennas at 3.5 GHz (a) without and; (b) with meta-surface.

showing the stability of the pattern over the whole operating frequency band. It can be observed that the cross polarization of the decoupled antenna is well suppressed within the entire frequency band of interest. Moreover, the radiation pattern after decoupling has also been improved in the xoz plane. Some other specific measured results are given in Table 3, illustrating the advantages of the proposed design.

Fig. 21 (a) shows the total efficiency of the antenna array, including the coupled antenna and the decoupled antenna. It can be observed that the measured efficiency of the decoupled antenna is increased from 85% to 90% compared to the

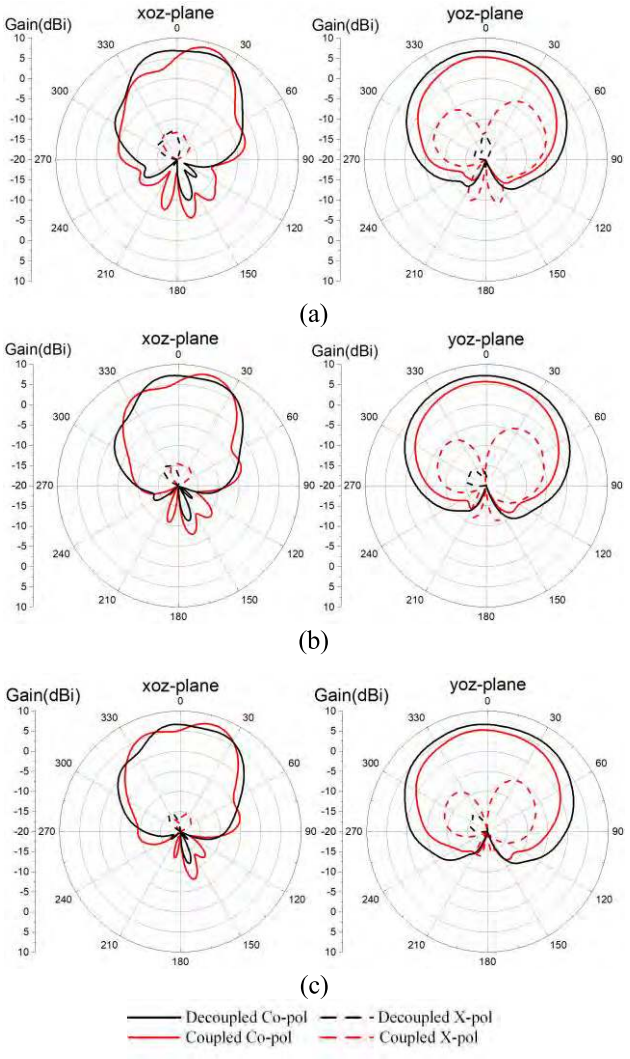

FIGURE 20. Measured radiation patterns of the antenna arrays without and with meta-surface: (a) at 3.3 GHz; (b) at 3.5 GHz; (c) at 3.7 GHz as port 1 is excited.

TABLE 3. Comparison of some specific values of the proposed antenna and initial antenna about radiation patterns (YOZ-Plane) with meta-surface.

Frequency	3.3 GHz	3.5 GHz	3.7 GHz
Gain	6.9 dBi	7.2 dBi	6.8 dBi
3 dB Beamwidth	114°	116°	116°
XPD	>20 dB	>19 dB	>20 dB
FBR	21.2 dB	24.4 dB	26.2 dB
Without Meta-surface			
Frequency	3.3 GHz	3.5 GHz	3.7 GHz
Gain	5.4 dBi	5.7 dBi	5.3 dBi
3 dB Beamwidth	87°	91°	97°
XPD	>5 dB	>6 dB	>8 dB
FBR	18.6 dB	20.4 dB	22.5 dB

coupled antenna at the center frequency of 3.5 GHz. The calculation results of the envelop correlation coefficient (ECC) of the antenna with and without meta-surface based on the measured patterns are given in Fig. 21 (b). The isolation of the antenna coupled in the E-plane before decoupling is already high, so the ECC of the array without meta-surface is small.

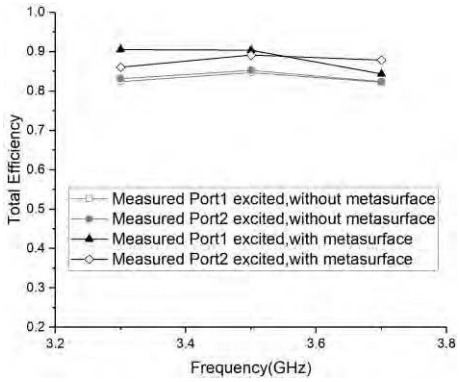

(a)

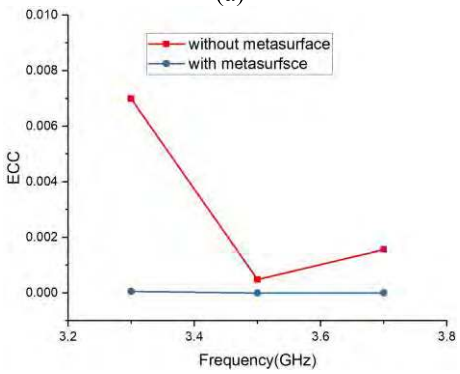

(b)

FIGURE 21. Measured (a) total efficiencies; and (b) ECCs for the two antennas without and with meta-surface.

TABLE 4. Comparison of the antenna arranged along the H-Plane and the antenna arranged along the E-Plane.

	antenna array 1	antenna array 2
hsub1	22 mm	21.3 mm
hgap	15 mm	8.2 mm
Bandwidth	3.2-3.65 GHz ($\|S_{11}\|$<-15 dB)	3.27-3.89 GHz ($\|S_{11}\|$<-15 dB)
Isolation	3.26-4 GHz ($\|S_{21}\|$<-25 dB)	3-3.97 GHz ($\|S_{21}\|$<-25 dB)
Gain	7±0.2 dBi	7±0.2 dBi

Nevertheless, the ECC of the decoupled antenna is still reduced with loading the meta-surface superstrate.

E. PERFORMANCE COMPARISON OF ANTENNAS IN TWO ARRANGEMENTS

A performance comparison between the antenna arranged along the H-plane (antenna array 1) and the antenna array arranged along the E-plane (antenna array 2), both with the meta-surface superstrate is listed in Table 4. As can be seen from it, antenna array 2 has a lower overall height than antenna array 1. Moreover, antenna array 2 has a wider impedance bandwidth. In terms of isolation, although antenna array 1 has higher isolation near the resonant frequency, antenna array 2 has a wider bandwidth for the isolation higher than 25 dB.

A comparison of the decoupling effect with recent works is shown in Table 5. As can be seen from it, the decoupling

TABLE 5. Comparison of the proposed antenna and reference antennas.

Ref.	Method	Freq. (GHz)	H-/E-Coup.	Distance (edge-to edge)	Enhancement of Isolation (dB)
[8]	Decoupling Network	2.45	H-	$0.055\lambda_c$	20.5
[14]	Defected Ground Structure	4.7	E-	$0.25\lambda_c$	10
[25]	Parasitic Elements	3.5	H-	$0.12\lambda_c$	25
[30]	EBG	5	H-	$0.22\lambda_c$	18
Prop.	Metasurface	3.5	H-	$0.05\lambda_c$	30.5
			E-	$0.011\lambda_c$	17.7

Here, λ_c represents the free-space wavelength at center frequency.

of the antennas arranged in one direction is studied in most papers. However, the decoupling of two antennas coupled in H- and E- plane is discussed in this paper respectively. Compared with [8], [25] and [30], the proposed antenna array arranged along the H-plane has a closer antenna spacing and a higher isolation at the center frequency. Moreover, the proposed antenna array arranged along the E-plane also has certain advantages in the antenna spacing and isolation improvement compared with [14].

IV. CONCLUSION

This paper introduces a decoupling method using meta-surface superstrates. The proposed meta-surface is composed of double layer short wires. By loading the meta-surface above two antennas coupled in H and E plane respectively, the isolation in both cases can reach to 25 dB under the premise of good matching at two ports for $|S_{11}| < -15$ dB in the band of operation (3.3 GHz −3.7 GHz). In addition, the gain at the boresight of the antenna array arranged in two directions both has been significantly improved. Through analyzing and comparing the antenna array arranged along the H-plane and the E-plane, it is known that this meta-surface can solve the decoupling problem of antenna array coupled not only in the H-plane but also in the E-plane. Therefore, this decoupling method is proved to be a promising candidate for base station antenna applications in the sub-6GHz region.

REFERENCES

[1] B. K. Lau, J. B. Andersen, G. Kristenson, and A. F. Molisch, "Impact of matching network on bandwidth of compact antenna arrays," *IEEE Trans. Antennas Propag.*, vol. 54, no. 11, pp. 3225–3238, Nov. 2006.
[2] Y.-F. Cheng and K.-K. M. Cheng, "A novel and simple decoupling method for a three-element antenna array," *IEEE Antennas Wireless Propag. Lett.*, vol. 16, pp. 1072–1075, 2017.
[3] S.-W. Su, C.-T. Lee, and F.-S. Chang, "Printed MIMO-antenna system using neutralization-line technique for wireless USB-dongle applications," *IEEE Trans. Antennas Propag.*, vol. 60, no. 2, pp. 456–463, Feb. 2012.
[4] L. Li, F. Huo, Z. Jia, and W. Han, "Dual zeroth-order resonance antennas with low mutual coupling for MIMO communications," *IEEE Antennas Wireless Propag. Lett.*, vol. 12, pp. 1692–1695, 2013.

[5] Y.-L. Ban, Z.-X. Chen, Z. Chen, K. Kang, and J. L.-W. Li, "Decoupled Hepta-band antenna array for WWAN/LTE smartphone applications," *IEEE Antennas Wireless Propag. Lett.*, vol. 13, pp. 999–1002, 2014.
[6] L. Zhao, L. K. Yeung, and K.-L. Wu, "A coupled resonator decoupling network for two-element compact antenna arrays in mobile terminals," *IEEE Trans. Antennas Propag.*, vol. 62, no. 5, pp. 2767–2776, May 2014.
[7] L. Zhao and K.-L. Wu, "A dual-band coupled resonator decoupling network for two coupled antennas," *IEEE Trans. Antennas Propag.*, vol. 63, no. 7, pp. 2843–2850, Jul. 2015.
[8] C.-H. Wu, C.-L. Chiu, and T.-G. Ma, "Very compact fully lumped decoupling network for a coupled two-element array," *IEEE Antennas Wireless Propag. Lett.*, vol. 15, pp. 158–161, 2016.
[9] H. Makimura, K. Nishimoto, T. Yanagi, T. Fukasawa, and H. Miyashita, "Novel decoupling concept for strongly coupled frequency-dependent antenna arrays," *IEEE Trans. Antennas Propag.*, vol. 65, no. 10, pp. 5147–5154, Oct. 2017.
[10] L. Zhao, F. Liu, X. Shen, G. Jing, Y.-M. Cai, and Y. Li, "A high-pass antenna interference cancellation chip for mutual coupling reduction of antennas in contiguous frequency bands," *IEEE Access*, vol. 6, pp. 38097–38105, 2018.
[11] Y.-F. Cheng and K.-K. M. Cheng, "A novel dual-band decoupling and matching technique for asymmetric antenna arrays," *IEEE Trans. Microw. Theory Techn.*, vol. 66, no. 5, pp. 2080–2089, May 2018.
[12] C.-M. Luo, J.-S. Hong, and L.-L. Zhong, "Isolation enhancement of a very compact UWB-MIMO slot antenna with two defected ground structures," *IEEE Antennas Wireless Propag. Lett.*, vol. 14, pp. 1766–1769, 2015.
[13] C.-T. Lee and K.-L. Wong, "Internal WWAN clamshell mobile phone antenna using a current trap for reduced ground plane effects," *IEEE Trans. Antennas Propag.*, vol. 57, no. 10, pp. 3303–3308, Oct. 2009.
[14] M. M. B. Suwailam, O. F. Siddiqui, and O. M. Ramahi, "Mutual coupling reduction between microstrip patch antennas using slotted-complementary split-ring resonators," *IEEE Antennas Wireless Propag. Lett.*, vol. 9, pp. 876–878, 2010.
[15] R. Anitha, V. P. Sarin, P. Mohanan, and K. Vasudevan, "Enhanced isolation with defected ground structure in MIMO antenna," *Electron. Lett.*, vol. 50, no. 24, pp. 1784–1786, 2014.
[16] S. Zhang, B. K. Lau, Y. Tan, Z. Ying, and S. He, "Mutual coupling reduction of two PIFAs with a T-shape slot impedance transformer for MIMO mobile terminals," *IEEE Trans. Antennas Propag.*, vol. 60, no. 3, pp. 1521–1531, Mar. 2012.
[17] J.-F. Li, Q.-X. Chu, Z.-H. Li, and X.-X. Xia, "Compact dual band-notched UWB MIMO antenna with high isolation," *IEEE Trans. Antennas Propag.*, vol. 61, no. 9, pp. 4759–4766, Sep. 2013.
[18] K. Wei, J.-Y. Li, L. Wang, Z.-J. Xing, and R. Xu, "Mutual coupling reduction by novel fractal defected ground structure bandgap filter," *IEEE Trans. Antennas Propag.*, vol. 64, no. 10, pp. 4328–4335, Oct. 2016.
[19] H. Li, Y. Tan, B. K. Lau, Z. Ying, and S. He, "Characteristic mode based tradeoff analysis of antenna-chassis interactions for multiple antenna terminals," *IEEE Trans. Antennas Propag.*, vol. 60, no. 2, pp. 490–502, Feb. 2012.
[20] H. Li, B. K. Lau, Z. Ying, and S. He, "Decoupling of multiple antennas in terminals with chassis excitation using polarization diversity, angle diversity and current control," *IEEE Trans. Antennas Propag.*, vol. 60, no. 12, pp. 5947–5957, Dec. 2012.
[21] H. Li, Z. T. Miers, and B. K. Lau, "Design of orthogonal MIMO handset antennas based on characteristic mode manipulation at frequency bands below 1 GHz," *IEEE Trans. Antennas Propag.*, vol. 62, no. 5, pp. 2756–2766, May 2014.
[22] H. Xu, H. Zhou, S. Gao, H. Wang, and Y. Cheng, "Multimode decoupling technique with independent tuning characteristic for mobile terminals," *IEEE Trans. Antennas Propag.*, vol. 65, no. 12, pp. 6739–6751, Dec. 2017.
[23] P. Liang and Q. Wu, "Characteristic mode analysis of antenna mutual coupling in the near field," *IEEE Trans. Antennas Propag.*, vol. 66, no. 7, pp. 3757–3762, Jul. 2018.
[24] X. Zhao, S. P. Yeo, and L. C. Ong, "Decoupling of inverted-F antennas with high-order modes of ground plane for 5G mobile MIMO platform," *IEEE Trans. Antennas Propag.*, vol. 66, no. 9, pp. 4485–4495, Jun. 2018.
[25] J.-Y. Deng, J.-Y. Li, and L.-X. Guo, "Decoupling of a three-port MIMO antenna with different impedances using reactively loaded dummy elements," *IEEE Antennas Wireless Propag. Lett.*, vol. 17, no. 3, pp. 430–433, Mar. 2018.
[26] L. Zhao and K.-L. Wu, "A decoupling technique for four-element symmetric arrays with reactively loaded dummy elements," *IEEE Trans. Antennas Propag.*, vol. 62, no. 8, pp. 4416–4421, Aug. 2014.
[27] K.-L. Wu, C. Wei, X. Mei, and Z.-Y. Zhang, "Array-antenna decoupling surface," *IEEE Trans. Antennas Propag.*, vol. 65, no. 12, pp. 6728–6738, Dec. 2017.
[28] F. Yang and Y. Rahmat-Samii, "Microstrip antennas integrated with electromagnetic band-gap (EBG) structures: A low mutual coupling design for array applications," *IEEE Trans. Antennas Propag.*, vol. 51, no. 10, pp. 2936–2946, Oct. 2003.
[29] M. J. Al-Hasan, T. A. Denidni, and A. R. Sebak, "Millimeter-wave compact EBG structure for mutual coupling reduction applications," *IEEE Trans. Antennas Propag.*, vol. 63, no. 2, pp. 823–828, Feb. 2015.
[30] X. Yang, Y. Liu, Y.-X. Xu, and S.-X. Gong, "Isolation enhancement in patch antenna array with fractal UC-EBG structure and cross slot," *IEEE Antennas Wireless Propag. Lett.*, vol. 16, pp. 2175–2178, 2017.
[31] M. M. Nikolic, A. R. Djordjevic, and A. Nehorai, "Microstrip antennas with suppressed radiation in horizontal directions and reduced coupling," *IEEE Trans. Antennas Propag.*, vol. 53, no. 11, pp. 3469–3476, Nov. 2005.
[32] M. Tang, Z. Chen, H. Wang, M. Li, B. Luo, J. Wang, Z. Shi, and R. W. Ziolkowski, "Mutual coupling reduction using meta-structures for wideband, dual-polarized, and high-density patch arrays," *IEEE Trans. Antennas Propag.*, vol. 65, no. 8, pp. 3986–3998, Aug. 2017.
[33] M. Farahani, J. Pourahmadazar, M. Akbari, M. Nedil, A. R. Sebak, and T. A. Denidni, "Mutual coupling reduction in millimeter-wave MIMO antenna array using a metamaterial polarization-rotator wall," *IEEE Antennas Wireless Propag. Lett.*, vol. 16, pp. 2324–2327, 2017.
[34] M. Akbari, H. A. Ghalyon, M. Farahani, A.-R. Sebak, and T. A. Denidni "Spatially decoupling of CP antennas based on FSS for 30-GHz MIMO systems," *IEEE Access*, vol. 5, pp. 6527–6537, 2017.
[35] Z. Wang, L. Y. Zhao Cai, S. Zheng, and Y. Yin, "A meta-surface antenna array decoupling (MAAD) method for mutual coupling reduction in a MIMO antenna system," *Sci. Rep.*, vol. 8, Feb. 2018, Art. no. 3152.
[36] F. Liu, J. Guo, L. Zhao, X. Shen, and Y. Yin, "A meta-surface decoupling method for two linear polarized antenna array in sub-6 GHz base station applications," *IEEE Access*, vol. 7, pp. 2759–2768, 2018.

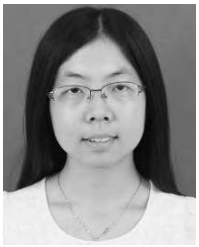

JIAYIN GUO received the B.S. degree in electronic information engineering from Xidian University, Xi'an, China, in 2016, where she is currently pursuing the Ph.D. degree in electromagnetic wave and microwave technology.

FENG LIU received the B.S. degree in electronic information engineering from Xidian University, Xi'an, China, in 2016, where he is currently pursuing the Ph.D. degree in electromagnetic wave and microwave technology.

LUYU ZHAO was born in Xi'an, China, in 1984. He received the B.Eng. degree from Xidian University, Xi'an, China, in 2007, and the Ph.D. degree from the Chinese University of Hong Kong, Hong Kong, in 2014.

From 2007 to 2009, he was with the Key Laboratory of Antennas and Microwave Technology, Xidian University, as a Research Assistant, where he was involved with software and hardware implementation of RF identification (RFID) technologies. From 2014 to 2015, he was a Postdoctoral Fellow with the Chinese University of Hong Kong. From October 2015 to October 2016, he was with Wyzdom Wireless Company Ltd., where he was a Co-Founder and CTO. He has been an Associate Professor with the National Key Laboratory of Antennas and Microwave Technology, Xidian University, since 2016. His current research interests include design and application of multiple antenna systems for next generation mobile communication systems, innovative passive RF and microwave components and systems, millimeter-wave and terahertz antenna array, and meta-material-based or inspired antenna arrays.

Dr. Zhao was a recipient of the Best Student Paper Award of 2013 IEEE 14th HK AP/MTT Postgraduate Conference, and the Honorable Mention Award of 2017 Asia-Pacific Conference on Antenna and Propagation. He is currently an Associate Editor for the journal IEEE Access.

YINGZENG YIN received the B.S., M.S., and Ph.D. degrees in electromagnetic wave and microwave technology from Xidian University, Xi'an, China, in 1987, 1990, and 2002, respectively. From 1990 to 1992, he was a Research Assistant and an Instructor with the Institute of Antennas and Electromagnetic Scattering, Xidian University, where he was an Associate Professor with the Department of Electromagnetic Engineering, from 1992 to 1996, and has been a Professor, since 2004. His current research interests include the design of microstrip antennas, feeds for parabolic reflectors, artificial magnetic conductors, phased array antennas, and computer-aided design for antennas.

GUAN-LONG HUANG (M'11–SM'18) received the B.E. degree in electronic information engineering from the Harbin Institute of Technology, Harbin, China, and the Ph.D. degree in electrical and computer engineering from the National University of Singapore, Singapore.

He was with the Temasek Laboratories, National University of Singapore, as a Research Scientist, and the Nokia Solutions and Networks System Technology, as a Senior Antenna Specialist, from 2011 to 2017. He is currently an Assistant Professor with the College of Information Engineering, Shenzhen University, Shenzhen, China. He also serves as the Deputy Director for the Guangdong Provincial Mobile Terminal Microwave and Millimeter-Wave Antenna Engineering Research Center. He has authored or coauthored more than 100 papers in journals and conferences. His research interests include design and implementation of planar antenna arrays, 5G base station and mobile RF front-end devices/antennas, phased antenna arrays, channel coding for massive MIMO applications, and 3D printing technology in microwave applications. He is serving as an Associate Editor for the journal IEEE Access.

YINGSONG LI received the B.S. degree in electrical and information engineering and the M.S. degree in electromagnetic field and microwave technology from Harbin Engineering University, China, in 2006 and 2011, respectively, and the Ph.D. degree from the Kochi University of Technology (KUT), Japan, and Harbin Engineering University, in 2014. He was a Visiting Scholar with the University of California, Davis, from March 2016 to March 2017. He has been a Full Professor with Harbin Engineering University, since July 2014. He is also a Visiting Professor with Far Eastern Federal University (FEFU) and KUT. His research interests include underwater communications, signal processing, compressed sensing, antenna, and antenna arrays. He is also a Senior Member of the Chinese Institute of Electronics (CIE). He is also an Associate Editor of IEEE Access and an Area Editor of the AEÜ—*International Journal of Electronics and Communications.* He also serves as a reviewer for more than 20 journals.